OAK RIDGE NATIONAL LABORATORY
operated by
UNION CARBIDE CORPORATION
for the
U.S. ATOMIC ENERGY COMMISSION

ORNL-TM-422

COPY NO. - 53

DATE - Dec. 3, 1962

A Monte Carlo Calculation of the Three-Dimensional Development of High-Energy Electron-Photon Cascade Showers

C. D. Zerby and H. S. Moran

Abstract

A description is given of a general-purpose Monte Carlo program for study of the three-dimensional development of high-energy electron-photon cascade showers in a homogeneous medium. The results of several study calculations are compared with previous analytic work to demonstrate the accuracy of the calculation. Another comparison with an experiment which measured the spatial distribution of the energy deposition in tin by 185-Mev electron-initiated showers shows a discrepancy between calculation and experiment.

Introduction

In the past few decades considerable interest has been generated in the theory of high-energy electron-photon cascade showers because of its use in analyzing cosmic-ray showers in air and emulsions. The advent of the high-energy electron accelerator has placed additional emphasis on the theory since it has applications in the design of accelerator equipment and experimental apparatus.

Many applications of the theory require extensive information about the three-dimensional development of the shower. Until recently, however, the analytic work on the theory dealt only with the longitudinal development of the shower. This work has been summarized by Rossi.[1] Previous Monte Carlo studies have also been limited to the one-dimensional development for simplicity. References to these calculations are given in a report by Zerby and Moran.[2]

Kamata and Nishimura[3] reported equations that could be solved numerically to obtain the lateral and angular distribution of a shower as a function of depth in an infinite medium. These equations resulted from extensive analytic work in which several approximations were made. Most of them introduce inaccuracies in the low-energy components of the shower.

The present calculation solves the three-dimensional shower problem by using the Monte Carlo method of computation. It was designed to have as few approximations as possible so that it would be applicable to relatively low energies (a few Mev). In addition, it was designed to consider any transporting medium with any elemental mixture in various geometrical configurations such as slabs, cylinders, and cylindrical shells. To increase its versatility, positrons and electrons are treated separately in the calculation.

---

1. B. Rossi, High-Energy Particles, Prentice-Hall, Englewood Cliffs, New Jersey (1952).
2. C. D. Zerby and H. S. Moran, Studies of the Longitudinal Development of High-Energy Electron-Photon Cascade Showers in Copper, ORNL-3329 (1962).
3. K. Kamata and J. Nishimura, Progr. Theoret. Phys. (Kyoto) 6, 93 (1958).

Approximating the Physical Processes

The basic approximations introduced in high-energy shower theory have been described previously[1-4] and will not be repeated here. It is important to note, however, that only a few of the physical processes possible need be included in the calculation to obtain accurate information about the shower. The energy degradation and transport of the photons are accurately treated if only pair production and Compton events are allowed. For the electrons and positrons, only radiative collisions and Coulomb collisions with the bound atomic electrons and the nucleus are required for accuracy. The remaining interactions can be neglected because the cross sections for their occurrence are small compared with those for the processes retained in the calculation.

Compton scattering is the only mechanism retained in the calculation by which the photon changes direction and contributes to the lateral and angular spread of the shower. The charged particles change directions by Coulomb scattering from the nucleus and the bound atomic electron and by radiative collisions. As pointed out by Rossi and Greisen,[4] however, the ratio of the root-mean-square angle of deflection of charged particles by nuclear Coulomb scattering in one radiation length to the average angle of emission in radiative collisions is approximately 40 to 1. Hence, no significant error is introduced if the angular deflections in radiative collisions are neglected. A parallel argument applies for neglecting the angular spread of the pairs produced in pair production by photons.

Cross Sections

The differential and total cross sections for pair production, Compton scattering, and bremsstrahlung were treated in this calculation as described by Zerby and Moran.[2] In all cases the correct energy dependence of the cross sections was used, in contrast to the asymptotic forms used in the analytic studies. In addition, screening effects

---

4. B. Rossi and K. Greisen, Rev. Mod. Phys. 13, 240 (1941).

were included in the expressions for pair production and bremsstrahlung. The Bethe-Heitler cross section for pair production, using the Born approximation, was modified further to correct for distortion of the electron wave functions in the electrostatic field of the nucleus. This correction is most important for the heavy elements at high energies, where the Bethe-Heitler expression underestimates the true cross section by as much as 10%.

The cross sections for each interaction were introduced into the calculation as equations or tables in such a way that the cross section could be obtained for any material with an elemental composition of less than twenty-one elements.

Small-Angle Scattering of the Charged Particles

It is not practical to treat the Coulomb scattering from the nucleus and the bound atomic electrons by the charged particles in the shower entirely as individual events in the Monte Carlo calculation. The charged particles experience far too many of these interactions as they travel from one point to another. The method adopted for handling this problem was to separate the large-angle Coulomb scattering from the small-angle Coulomb scattering and to treat them independently. Analytic results for the lateral and angular deflection of a charged particle caused by multiple small-angle deflections were used to account for the small-angle Coulomb scattering, while large-angle scatterings were treated as individual events. One advantage of this approach is that proper account can be taken of those bound atomic electrons given enough energy in ionization collisions to become part of the shower.

The angle that separates the small-angle Coulomb scattering from the large-angle Coulomb scattering was dictated to a certain extent by the analytic solution used for small-angle multiple scattering. The demonstration of this dependence first requires a consideration of the equation used to represent the Coulomb scattering at small angles.

The cross section for positron or electron scattering from the nucleus in the limit $E \gg mc^2$ and for small angles without screening is given by

$$d\sigma = 8\pi NZ^2 \, r_e^2 \left(\frac{mc^2}{E}\right)^2 \frac{d\theta}{\theta^3}, \qquad (1)$$

where N is the nuclear density, r_e is the classical electron radius, and θ is the polar angle of scattering. This equation must be modified to include small-angle scattering from the atomic electrons and screening effects. The scattering from the atomic electrons can be accounted for approximately by replacing the factor Z^2 by $Z(Z + 1)$ in Eq. 1, and the screening effects can be accounted for approximately by using $V = Ze^2 r^{-1} \exp(-r/a)$, where $a = \hbar^2 Z^{-1/3}/mc^2$, for the electrostatic field of the atom in the modification of the derivation of Eq. 1 as described by Goudsmit and Saunderson.[5] The result of both these modifications is the expression

$$d\sigma = 8\pi N \, Z(Z + 1) \, r_e^2 \left(\frac{mc^2}{E}\right)^2 \frac{\theta d\theta}{(\theta^2 + \theta_1^2)^2}, \qquad (2)$$

where $\theta_1 = Z^{1/3} \alpha(mc^2/E)$ and $\alpha = 1/137$. Equation 2 applies only for small angles of scattering, say, $0 \leq \theta \leq \theta_m$.

The root-mean-square angle of scattering from Eq. 2 in the range $0 \leq \theta \leq \theta_m$, which will be useful later, is given by

$$\langle\theta^2\rangle = 4\pi NZ(Z + 1) \, r_e^2 \left(\frac{mc^2}{E}\right)^2 \left\{ \ell n \left[\left(\frac{\theta_m}{\theta_1}\right)^2 + 1\right] - 1 + \frac{\theta_1^2}{(\theta_1^2 + \theta_m^2)} \right\}. \qquad (3)$$

The analytic solution to the multiple small-angle scattering problem used in the calculation was the one obtained by Eyges[6] as a modification of the derivation by Fermi.[1,4] Fermi first obtained a solution to an approximate charged-particle transport equation that is applicable for small-angle multiple scattering and gives the joint distribution

---

5. S. A. Goudsmit and J. L. Saunderson, Phys. Rev. 57, 24 (1940) and Phys. Rev. 58, 36 (1940).
6. L. Eyges, Phys. Rev. 74, 1534 (1948).

function for the lateral and angular spread of a charged particle beam as a function of depth. The basic approximations in the formulation of the transport equation were that only small angular deviations from the initial direction of the beam occurred, no energy loss need be considered, and only scattering interactions took place. In addition, however, the Landau approximation[3] was made in the scattering term of the transport equation. The modification made by Eyges was to obtain the first-order solution to the same equation which included constant energy loss by ionization collisions. The joint-distribution function derived by Eyges* is

$$f(z,x,\theta_x)\ dx\ d\theta_x = \frac{dx\ d\theta_x}{4\pi B} \exp\left(\frac{-A_2\theta_x^2 + 2A_1 x\theta_x - A_0 x^2}{4B}\right), \qquad (4)$$

where

$$A_n(z) = \int_0^z \frac{(z - z')^n\, dz'}{W^2(z')} \quad \text{for } n = 0,1,2 \qquad (4a)$$

$$W^2(z) = 4/\langle\theta^2\rangle, \qquad (4b)$$

$$B(z) = A_0(z)\ A_2(z) - A_1^2(z). \qquad (4c)$$

In Eq. 4 the distance along the z axis, which coincides with the original direction of the beam, is given by z, and θ_x is the projection on the x axis of a unit vector along the direction of angular deflection under the assumption that the polar angle of deflection is small. The quantity $\langle\theta^2\rangle$ in Eq. 4b is the root-mean-square polar angle of scattering. The independent distribution function $f(z,y,\theta_y)$ is obtained from Eq. 4 by replacing x with y. The lateral displacement is given by $r = (x^2 + y^2)^{1/2}$, and the polar angle by $\theta = (\theta_x^2 + \theta_y^2)^{1/2}$.

---

*The equations presented by Eyges[6] contained several typographical errors. These have been corrected in the present paper.

There are difficulties with Eyges' solution, however, because of the use of the Landau approximation in the transport equation. The distribution function for θ_x, which is obtained from Eq. 4 by integrating over all values of x, actually falls below the single-scattering estimate at thickness z for large values of θ_x. This is clearly impossible. Use of the Landau approximation would become more valid, however, if the scattering cross section did not include a large-angle contribution. This suggests the criteria for separating the large-angle scattering from small-angle scattering that was referred to previously.

Letting θ_m be a small angle forming a boundary between small-angle and large-angle single scattering, which means it is also the maximum angle of small-angle scattering considered in Eyges' derivation, then we expect Eq. 4 to be accurate for angles in the distribution function less than approximately θ_m. For angles greater than θ_m the distribution function is supplemented by the large-angle single-scattering events. For an average distance traveled of length z at least one large-angle single scattering is required to contribute to the distribution function to assure accuracy. Hence,

$$1 \lesssim z \int_{\theta_m}^{\infty} \frac{d\sigma}{d\theta}\, d\theta, \tag{5}$$

where $d\sigma/d\theta$ is the differential cross section for large-angle scattering. By using Eq. 1 for the large-angle scattering in Eq. 5,

$$\theta_m \leq \left(\frac{zQ}{2}\right)^{1/2}, \tag{6}$$

where $Q = 8\pi NZ^2 r_e^2 (mc^2/E)^2$. The average distance traveled, z, in this process is approximately the mean free path for bremsstrahlung events, which can be determined from the asymptotic form of the bremsstrahlung cross section. When that distance is used, an acceptable value for θ_m is $2.8\ (mc^2/E)$. With the aid of this value of θ_m, Eq. 3 now becomes

$$\langle\theta^2\rangle = \frac{4P}{E^2} , \tag{7}$$

where the condition $\theta_1/\theta_m \ll 1$ was used to simplify the equation, and $P = 2\pi NZ(Z + 1)\ r_e^2(mc^2)^2\ [\ell n(2.8 \times 137\ Z^{-1/3}) - 1/2]$.

The root-mean-square angle of scattering is made a function of z by introducing the stopping power for ionization collisions, ν, which is assumed to be constant over short distances involved, so that

$$\langle\theta^2\rangle = \frac{4P}{(E - \nu z)^2} . \tag{7a}$$

Equation 7a was substituted into Eq. 4a to obtain

$$A_0(z) = \frac{Pz}{E(E - \nu z)} , \tag{8a}$$

$$A_1(z) = \frac{P}{\nu^2}\left[\ell n\left(\frac{E}{E - \nu z}\right) - \frac{\nu z}{E}\right] , \tag{8b}$$

$$A_2(z) = \frac{P}{\nu^2}\left[2z - \frac{\nu z^2}{E} - \frac{2(E - \nu z)}{\nu}\ell n\left(\frac{E}{E - \nu z}\right)\right] , \tag{8c}$$

which completely specify the functions needed in the distribution function given in Eq. 4.

The stopping power for ionization collisions required in the above derivation is not the usual one, because the large-angle scatterings are treated as individual events in this calculation and therefore should not make a contribution to the continuous energy degradation characterized by the stopping power ν. This is discussed below.

Large-Angle Scattering of the Charged Particles

It was most convenient to use Eq. 1 for large-angle Coulomb scattering from the nucleus even though it is accurate for small-angle scattering only. The minumum angle to which it applies is $\theta_m = 2.8\ (mc^2/E)$. At larger angles Eq. 1 must be modified because the structure of the nucleus affects the scattering, tending to reduce it appreciably as θ becomes larger than $\theta_2 = 280A^{1/3}\ (mc^2/E)$. Along with Williams,[7] we make the approximation that the cross section is zero for $\theta > \theta_2$. If $\theta_2 > \pi$, then the cross section is set equal to zero for $\theta > \pi$.

For large-angle charged-particle collisions with the atomic electrons the free electron-electron cross section derived by Møller[8] and the free positron-electron cross section derived by Bhabha[9] are used. These cross sections are given by

$$\frac{d\sigma}{dx} = 2\pi NZr_e^2 \frac{(\epsilon + 1)^2}{\epsilon^2(\epsilon + 2)} \left[\frac{1}{x^2} - \frac{(2\epsilon + 1)}{x(1 - x)(\epsilon + 1)^2} + \frac{1}{(1 - x)^2} + \frac{\epsilon^2}{(\epsilon + 1)^2}\right],$$

$$x_m \leq x \leq 1/2, \qquad (9)$$

for electrons and

$$\frac{d\sigma}{dx} = 2\pi NZr_e^2 \frac{(\epsilon + 1)}{x^2\ \epsilon^2} \left\{\frac{1}{(\epsilon + 2)(\epsilon + 1)} \left[(\epsilon + 1)^2 - \frac{(2\epsilon^2 + 8\epsilon + 5)\epsilon x}{\epsilon + 2}\right.\right.$$

$$\left.\left. + \frac{(3\epsilon^2 + 12\epsilon + 13)(\epsilon x)^2}{(\epsilon + 2)^2} + \frac{2(\epsilon + 1)(\epsilon x)^3}{(\epsilon + 2)^2} + \frac{(\epsilon x)^4}{(\epsilon + 2)^2}\right]\right\},$$

$$x_m \leq x \leq 1, \qquad (10)$$

---

7. E. J. Williams, Proc. Roy. Soc. A169, 531 (1939).
8. C. Møller, Ann. Physik 14, 531 (1932).
9. H. J. Bhabha, Proc. Roy. Soc. A154, 195 (1936).

for positrons. In these equations ϵ is the kinetic energy of the incident particle, in mc^2 units, and x is the fraction of the incident kinetic energy transmitted to the target particle. The cosines of the polar angles of ejection in these processes are given by

$$\mu_1 = \left[\frac{x(\epsilon + 2)}{\epsilon x + 2} \right]^{1/2}, \tag{11a}$$

and

$$\mu_2 = \left[\frac{(1 - x)(\epsilon + 2)}{\epsilon(1 - x) + 2} \right]^{1/2}, \tag{11b}$$

where μ_1 refers to the electron and μ_2 to the positron in positron-electron scattering. They both refer to the electrons in electron-electron scattering.

The smallest value of x_m allowed in Eqs. 9 and 10 is determined from Eq. 11b by using θ_m as the smallest polar angle of scattering. This results in $x_m = (2.8)^2/2\epsilon$, when $\theta_m \ll 1$ and $\epsilon \gg 2.8$ are employed to simplify the equation. This means that all atomic electrons given an energy greater than ~ 2 Mev in electron-electron or positron-electron collisions are added to the cascade.

Stopping Power for Ionization Collisions

As pointed out previously, since the large-angle electron-electron scattering and positron-electron scattering are treated as individual events, the energy degradation attributed to them must be subtracted from the usual form of the stopping-power expression for ionization collisions.[10] When this is done and $x_m \ll 1$ is used, then

$$\nu \equiv -\frac{dE}{dx} = 2\pi NZr_e^2 mc^2 \left\{ \ell n \left[\frac{E^2(2.8)^2}{I^2} \right] - 1 \right\} \tag{13}$$

---

10. E. A. Uehling, Ann. Rev. Nucl. Sci. 4, 315 (1956).

for both positrons and electrons, where E is the total energy of the particle and I is the average ionization potential.[10]

The Monte Carlo Procedure

The Monte Carlo procedure for treating the photons was straightforward. For each photon that appeared in the cascade the total macroscopic cross section, Σ_γ, which was the sum of the pair production and Compton cross sections, was calculated for the medium being studied. The distance to the next collision point, x, was selected from the exponential distribution, $\Sigma_\gamma \exp(-\Sigma_\gamma x)$. At the point of interaction the choice between a pair-production event and a Compton event was made in the standard way.

If a pair-production event occurred at the point of collision, then the partition of energy between the positron and the electron was determined by a random selection technique, and both members were added to the cascade. These particles were directed along the incident direction of the photon. If a Compton event took place, the degraded energy of the photon was selected from the Klein-Nishina distribution function and the new direction of the degraded photon determined. The Compton-ejected electron was also added to the cascade, with energy and direction determined from the kinematics of the collision.

For each charged particle that appeared in the cascade the total macroscopic cross section, Σ_c, which was the sum of the cross sections for bremsstrahlung, large-angle nuclear Coulomb scattering, and large-angle Coulomb scattering from the atomic electrons, was calculated from tables or equations for the medium under study. The distance to the next collision point, z, was then selected in an appropriate manner, using that cross section. If the cross sections were constant, then the selection would be from out of an exponential distribution as in the case of photons; however, Σ_c changes with distance as the charged particle loses energy by ionization collisions, and a special technique had to be devised to treat this problem.

Having selected the distance traveled, z, the lateral and angular deviation of the charged particle by small-angle Coulomb collisions were selected from the joint distribution functions $f(z,x,\theta_x)$ and $f(z,y,\theta_y)$ described in Eq. 4, and the new particle energy was determined by using the stopping-power formula for the medium. The collision point of the particle was then shifted by the distance $r = (x^2 + y^2)^{1/2}$, and the direction of the particle was rotated through the polar angle $\theta = (\theta_x^2 + \theta_y^2)^2$.

At the point of interaction the type of interaction was selected in a standard manner. For a bremsstrahlung event the partition of the energy between the photon and the charged particle was selected with the appropriate probability and the two were added to the cascade. The angular deflection for large-angle Coulomb scattering from the nucleus was determined from a selection technique based on Eq. 1. The selection techniques for large-angle scattering from the atomic electrons were based on Eqs. 9 and 10. In these processes the incident particle was allowed to change direction and lose energy. The direction and energy of the atomic electron were also calculated from the kinematics of the collision and added to the cascade.

The Computer Program

The present version of the computer program, which was written for the IBM-7090, will develop cascades in a homogeneous material with mixtures of up to 20 elements. The composition is specified by input to the program, and the cross sections are set up automatically. The geometrical configuration of the medium can be a slab, cylinder, or cylindrical shell, as specified by input to the program. The cascades can be initiated by normally incident positrons, electrons, or photons at any incident energy up to 50 Gev.

One feature of the program is the variable nature of the energy bounds for spectral data. It is possible to arbitrarily select up to 15 such bounds other than the source energy, thus dividing the spectral data into the corresponding number of intervals. In addition, eight radial bounds can be specified which divide the scattering medium into

cylindrical shells. The depth in the medium is automatically divided into half-radiation-length-thick layers out to 10 radiation lengths.

The results of the calculation include data on the track length[2] for charged particles and for photons in each energy interval, radial interval, and depth interval. Fluxes of charged particles and of photons are also given in each energy interval at each radiation length of depth out to a depth of 10 radiation lengths. The calculation also provides the energy deposited in each depth interval and radial interval and provides the energy spectra and angular distribution of the radiation penetrating the scattering medium if the medium has a finite thickness.

Study Calculations

A series of calculations were performed with this new program to compare the results with the analytic formula derived by Fermi[1,4] and the results reported by Snyder and Scott[11] and discussed by Rossi.[1] In making these comparisons it is important to note the differences in the way the problems were formulated in order to properly evaluate the differences that might appear.

Although the Fermi and Snyder-Scott results were both limited to the case of electron transport without generation and transport of photons and without energy degradation of the electrons, they differed in two respects. First, the Fermi approach used the Landau approximation while the Snyder-Scott approach did not. Thus, one would expect differences in the results from the two studies at large angles of scattering where the Snyder-Scott solution would usually be more accurate. At these large angles the Fermi distribution usually gives an underestimate of the correct result and, in fact, falls below the single-scattering estimate, as does Eyges' solution as pointed out previously. Second, they differ in the way the Coulomb scattering was treated. Fermi used Eq. 1 for the differential cross section for Coulomb scattering with the restriction that the cross section was zero for $\theta < \theta_1 = Z^{1/3}\,\alpha(mc^2/E)$ and for $\theta > \theta_2 = 280\,A^{-1/3}\,(mc^2/E)$, and Snyder and Scott used Eq. 2 for the cross section and placed no restriction on the maximum angle of scattering.

---

11. H. S. Snyder and W. T. Scott, Phys. Rev. 75, 220 (1949).

The Fermi joint distribution function for the lateral and angular spread of the electrons which corresponds to Eq. 4 is

$$f(z,x,\theta_x)\ dx\ d\theta_x = \frac{dx\ d\theta_x\ W^2\sqrt{3}}{2\pi z^2} \exp\ \left[-W^2\left(\frac{\theta_x^2}{z} - \frac{3x\theta_x}{z^2} + \frac{3x^2}{z^3}\right)\right], \quad (14)$$

where

$$\frac{\langle\theta^2\rangle}{4} = \frac{1}{W^2} = 2\pi NZ^2 r_e^2 \left(\frac{mc^2}{E}\right)^2 \quad \ell n\ \frac{\theta_2}{\theta_1}\ .$$

Equation 14 can be integrated over all values of the lateral distance x $(-\infty < x < +\infty)$ to obtain the angular distribution given by

$$g(s,\eta)\ d\eta = d\eta(p^2 s\pi)^{-1/2}\ \exp(-\eta^2/p^2 s), \quad (15)$$

where

$$\eta = \theta_x/\theta_1,$$

$$s = z/X_s,$$

$$1/X_s = 4\pi N(137\ r_e)^2\ Z^{4/3},$$

$$p^2 = 2\ell n(\theta_2/\theta_1) = 2\ell n(137 \times 280 \times A^{-1/3}\ Z^{-1/3}).$$

Alternately, Eq. 14 can be integrated over all values of the angle θ_x $(-\infty < \theta_x < +\infty)$ to obtain the lateral distribution given by

$$k(s,\beta_x)\ d\beta_x = d\beta_x\left(\frac{1}{3}\ p^2 s\pi\right)\ \exp\ \left(-3\beta_x^2/p^2 s\right)\ , \quad (16)$$

where $\beta_x = x/z\theta_1$.

In the comparisons of the angular distributions from the various calculations it was of interest to display the distribution function for single scattering. The required single-scattering function to be compared with Eq. 15, for example, was obtained from Eq. 1 after multiplying by the thickness z. By requiring that the maximum polar angle of scattering be equal to θ_2 in the revised Eq. 1, changing variables to θ_x and θ_y using the substitutions $\theta = (\theta_x^2 + \theta_y^2)^{1/2}$ and $\theta\, d\theta = (2\pi)^{-1}\, d\theta_x\, d\theta_y$, and integrating over the allowed range of θ_y, the required single-scattering function is obtained as

$$g(s,\eta)\, d\eta = \frac{d\eta s}{\pi\eta^3}\left\{ \frac{\eta\left[(\theta_2/\theta_1)^2 - \eta^2\right]^{1/2}}{(\theta_2/\theta_1)^2} + \tan^{-1}\left[\frac{(\theta_2/\theta_1)^2 - \eta^2}{\eta^2}\right]^{1/2}\right\}. \tag{17}$$

To make the results of the present calculation more comparable with the analytic results of Fermi and Snyder and Scott, the program was altered so that no bremsstrahlung radiation was produced and the electrons did not change energy by ionization collisions. Under the assumption of no energy degradation, Eq. 4, which includes only small-angle scattering, reduces to the form of the Fermi solution given in Eq. 14 with the exception that

$$1/W^2 = 2\pi NZ(Z + 1)r_e^2 \left[\ell n(2.8 \times 137\, Z^{-1/3}) - 1/2\right].$$

Hence, the angular distribution and lateral distribution which include only small-angle scattering are given by Eqs. 15 and 16, respectively, except that

$$p^2 = 2\,\frac{(Z + 1)}{Z}\left[\ell n(2.8 \times 137\, Z^{-1/3}) - 1/2\right].$$

These solutions will be referred to as Fermi's solutions including only small-angle scattering.

Figures 1 and 2 show a comparison of the angular distributions from the various calculations for the case of 100-Mev electrons incident on beryllium (density 1.8). To obtain the distribution functions in the present work the problem was calculated in three dimensions, and the unit vector along the direction of the particle at the exit surface of the slab was projected on to the x axis to obtain θ_x. Figure 1 is for a target thickness s = 100 (0.01258 g/cm^2), and Fig. 2 is for s = 84,000 (10.57 g/cm^2).

In Figs. 1 and 2 it will be noticed that the Snyder-Scott distribution is greater than the single-scattering distribution at the larger angles, as the correct distribution should be, while the Fermi distribution drops below the single-scattering distribution at the larger angles. In Fig. 1 the Monte Carlo results tend to follow the Fermi solution which includes only small-angle scattering because the depth in beryllium is small, and large-angle scatterings are very improbable. At the larger angles in the distribution the Monte Carlo results are above the Fermi solution including only small-angle scattering but still seriously below the correct answer. The difficulty here is that an insufficient number of samples (only 2,000) were taken, and in such cases underestimates are very likely.

In Fig. 2 where a greater depth in beryllium is considered, the number of large-angle scatterings is significant and the Monte Carlo results properly reflect their effect on the distribution function which approximates the Snyder-Scott results very closely.

In the Monte Carlo calculation for the lateral spread of the beam it was more convenient to obtain an estimate of the radial distribution rather than the x or y distributions. For comparison the radial distribution can be obtained from the Fermi distribution given in Eq. 16 by noting that

$$k(s,\beta)\ \beta d\beta\ d\psi = k(s,\beta_x)\ k(x,\beta_y)\ d\beta_x\ d\beta_y$$

$$= \beta d\beta\ d\psi\ \left(\frac{1}{3}\, p^2 s\pi\right)^{-1} \exp\left(-3\beta^2/p^2 s\right), \qquad (18)$$

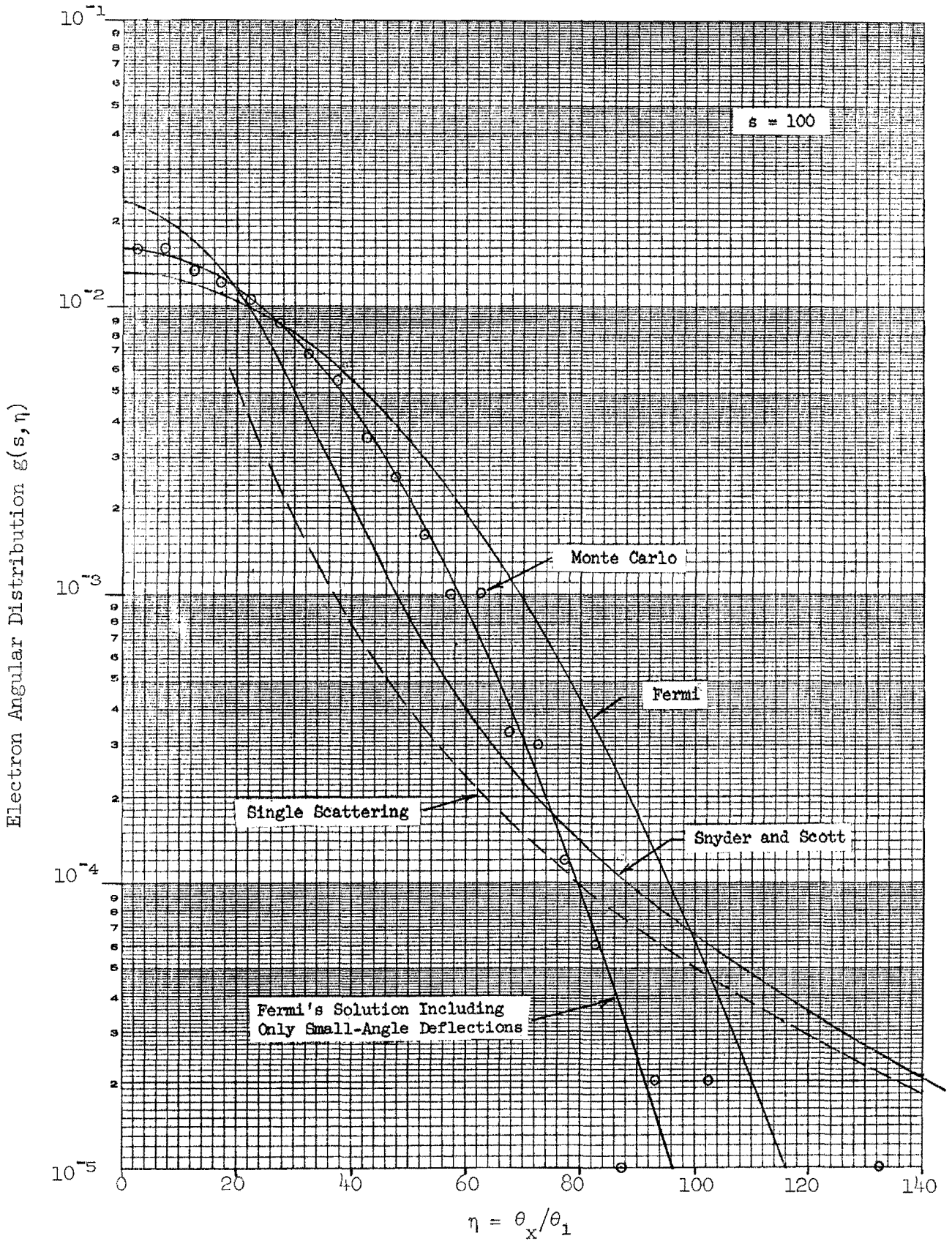

Fig. 1. Electron Angular Distribution in Beryllium at s = 100 (0.01258 g/cm^2) Resulting from a Monodirectional, 100-Mev Incident Beam of Electrons. Bremsstrahlung production and energy degradation by ionization collisions were not allowed.

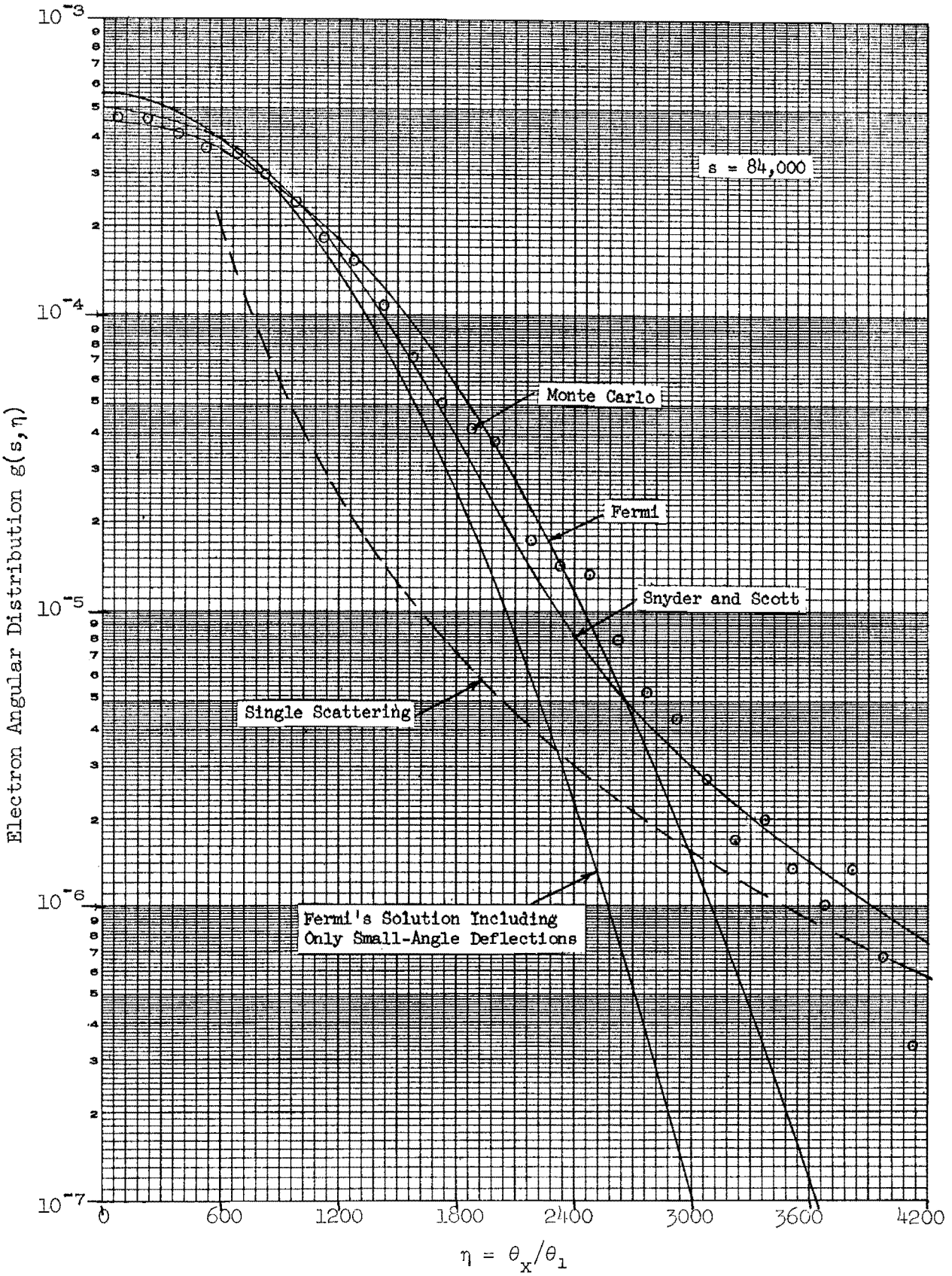

Fig. 2. Electron Angular Distribution in Beryllium at s = 84,000 (10.57 g/cm^2) Resulting from a Monodirectional, 100-Mev Incident Beam of Electrons. Bremsstrahlung production and energy degradation by ionization collisions were not allowed.

where $\beta = (\beta_x^2 + \beta_y^2)^{1/2}$ and ψ is the azimuthal angle.

Figures 3 and 4 present comparisons of the Monte Carlo results with the Fermi distributions for the beryllium cases just discussed. For the case of a small depth in beryllium shown in Fig. 3, the Monte Carlo results compare with the Fermi solution including only small-angle deflections as they did in the corresponding case for the angular distributions. At the larger depth shown in Fig. 4, the Monte Carlo results approach the Fermi solution. In the latter case, within the limits of the variable investigated, there is no evidence of the Monte Carlo distribution becoming greater than the Fermi distribution at large radial distances as might be suggested by the results shown in Fig. 2.

Figures 5 and 6 present the angular distribution from the various calculations for the case of 100-Mev electrons incident on lead (density 11.35). Figure 5 is for a target thickness s = 100 (0.005166 g/cm^2), and Fig. 6 is for s = 84,000 (4.339 g/cm^2). In Fig. 5 we see the Monte Carlo results following the Fermi solution including only small-angle scattering as the angle increases. At the larger angles the large-angle scattering clearly makes the Monte Carlo results tend toward the Snyder-Scott solution, although the statistical accuracy is very poor, as can be seen from the spread of the data points.

In Fig. 6 we see a more interesting situation. In this case the single-scattering distribution is cut off at $\eta = \theta_2/\theta_1 = 1492$ for lead because of the effect of the nucleus on the scattering distribution. Since the Snyder-Scott solution does not include the cutoff in the maximum angle of scattering, it is evident that it gives an overestimate of the large-angle contributions to the distribution function. The Fermi solution, on the other hand, does include the cutoff and should be more accurate. As can be seen in Fig. 6, the Monte Carlo results approximate the Fermi solution very well, as they should since the Monte Carlo solution also includes the cutoff.

A comparison of the Monte Carlo and Fermi radial distributions in the lead cases indicates an agreement similar to that shown in Figs. 3 and 4.

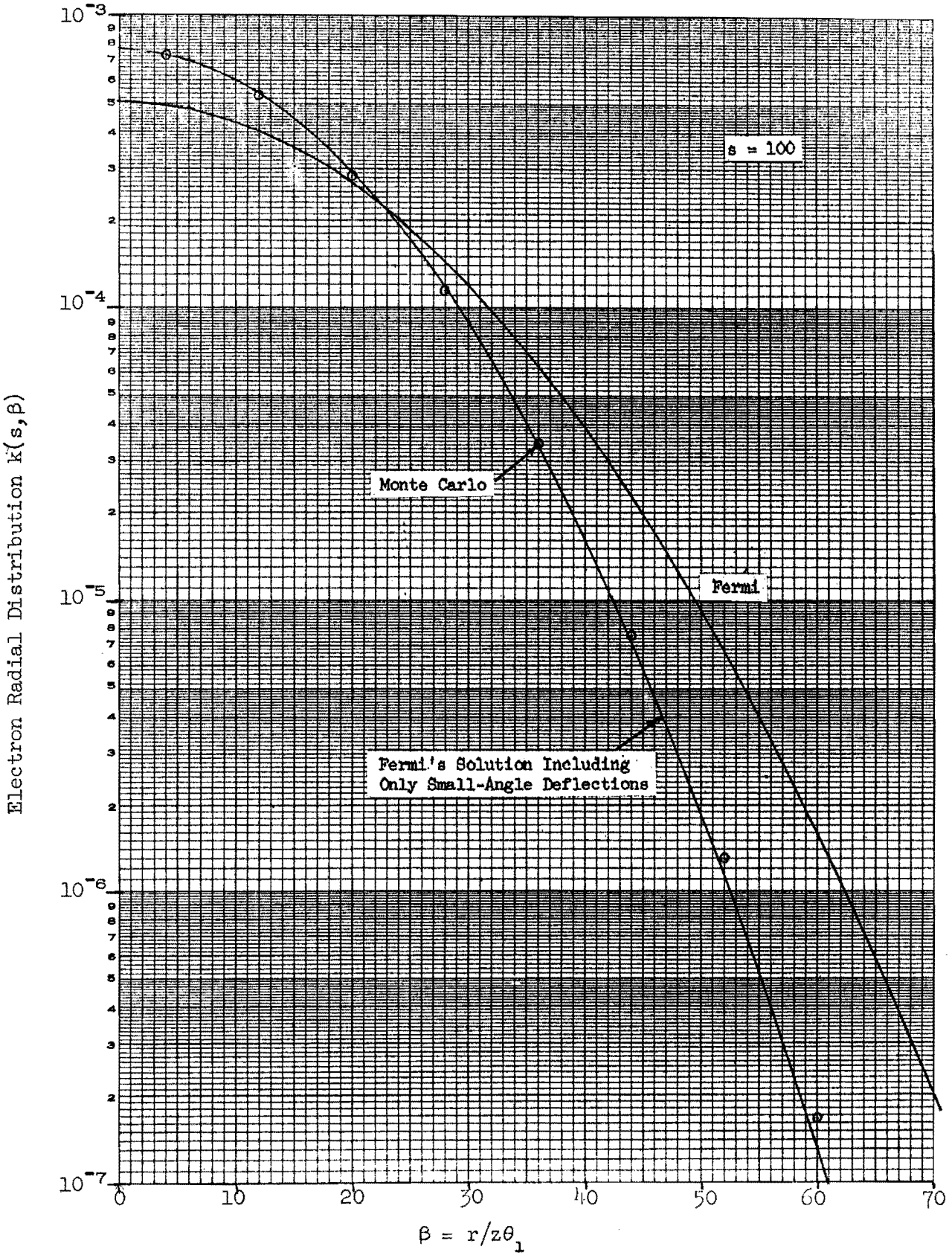

Fig. 3. Electron Radial Distribution in Beryllium at s = 100 (0.01258 g/cm^2) Resulting from a Monodirectional, 100-Mev Incident Beam of Electrons. Bremsstrahlung production and energy degradation by ionization collisions were not allowed.

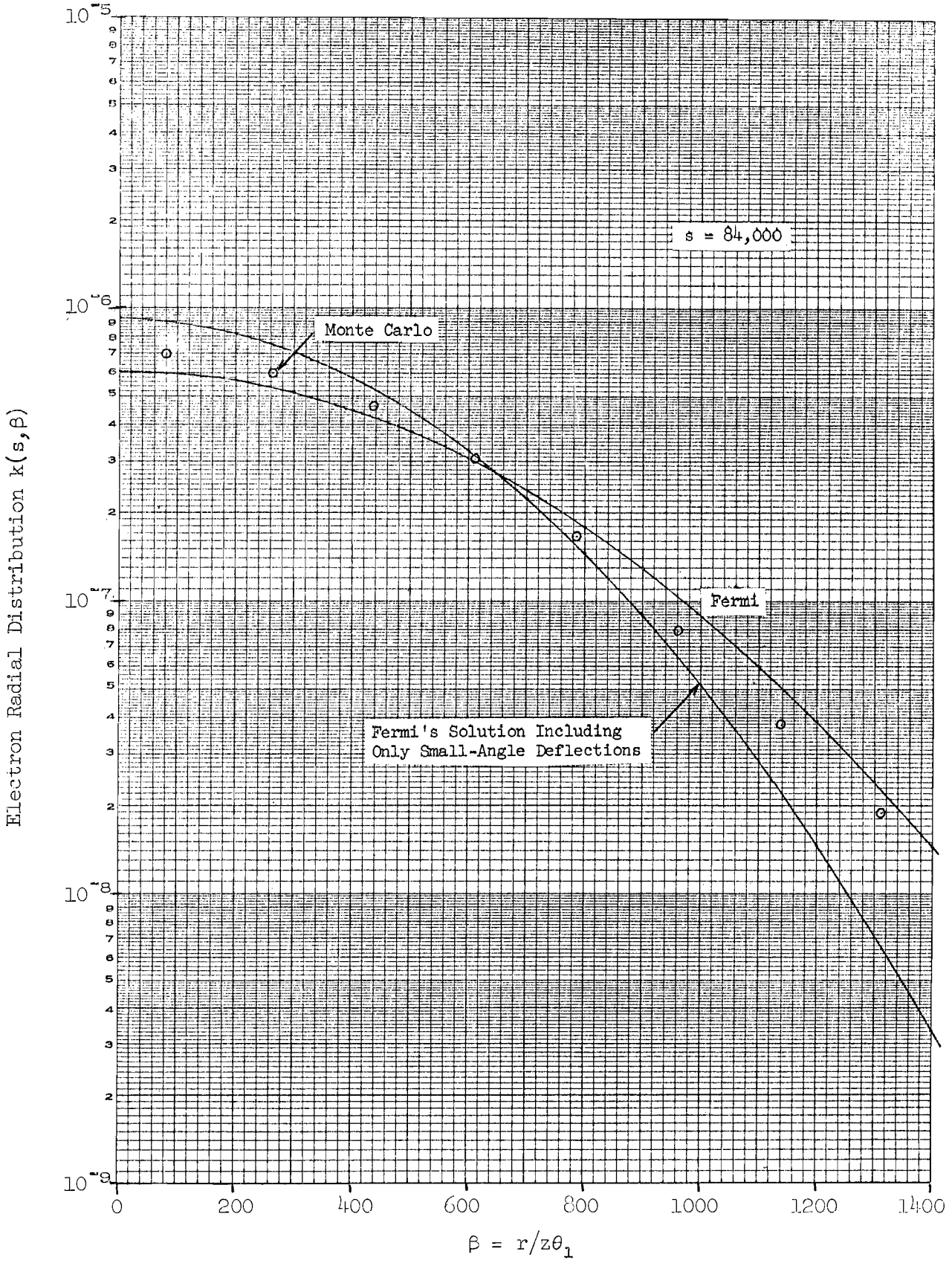

Fig. 4. Electron Radial Distribution in Beryllium at s = 84,000 (10.57 g/cm^2) Resulting from a Monodirectional, 100-Mev Incident Beam of Electrons. Bremsstrahlung production and energy degradation by ionization collisions were not allowed.

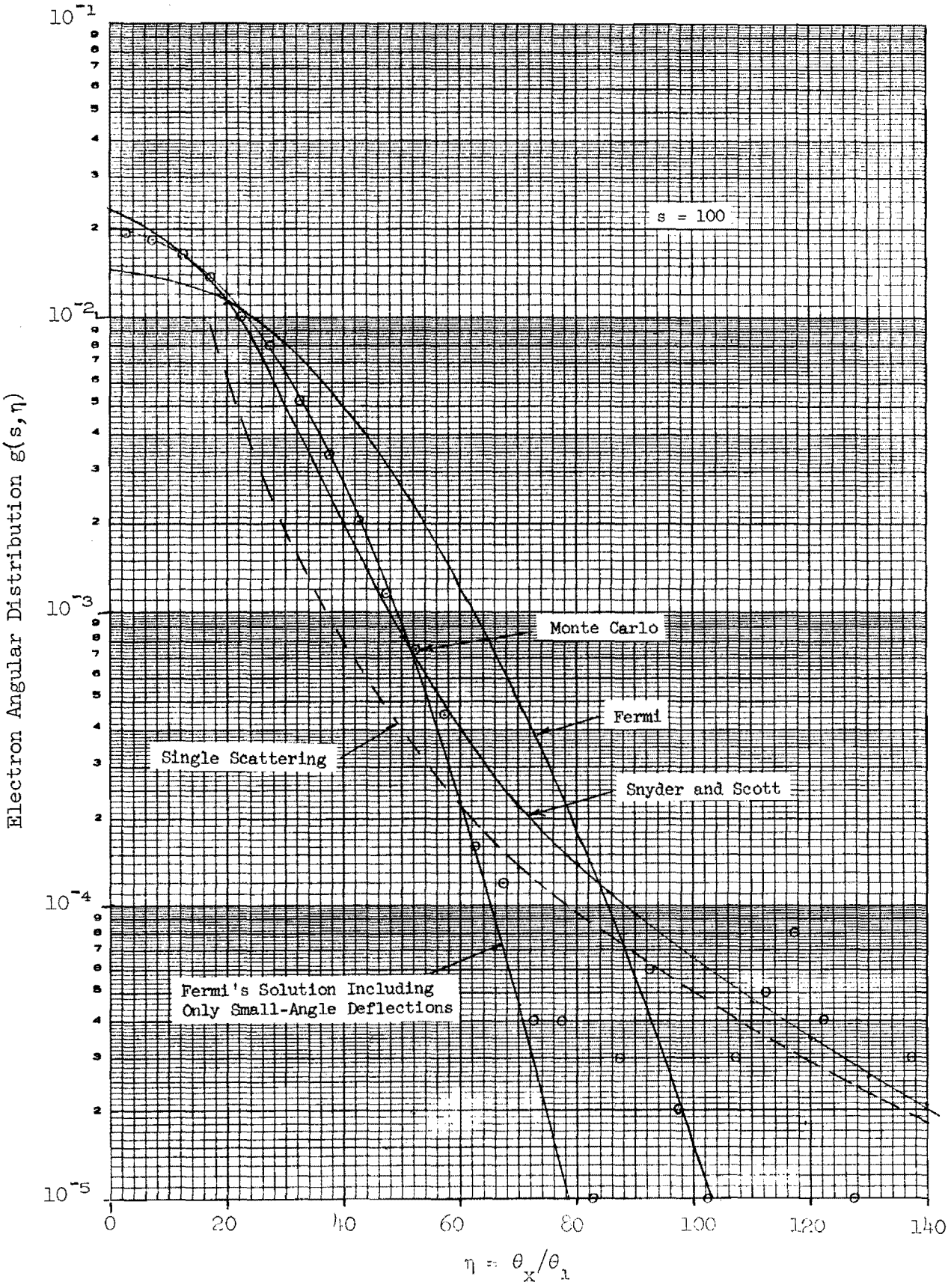

Fig. 5. Electron Angular Distribution in Lead at s = 100 (0.005166 g/cm^2) Resulting from a Monodirectional, 100-Mev Incident Beam of Electrons. Bremsstrahlung production and energy degradation by ionization collisions were not allowed.

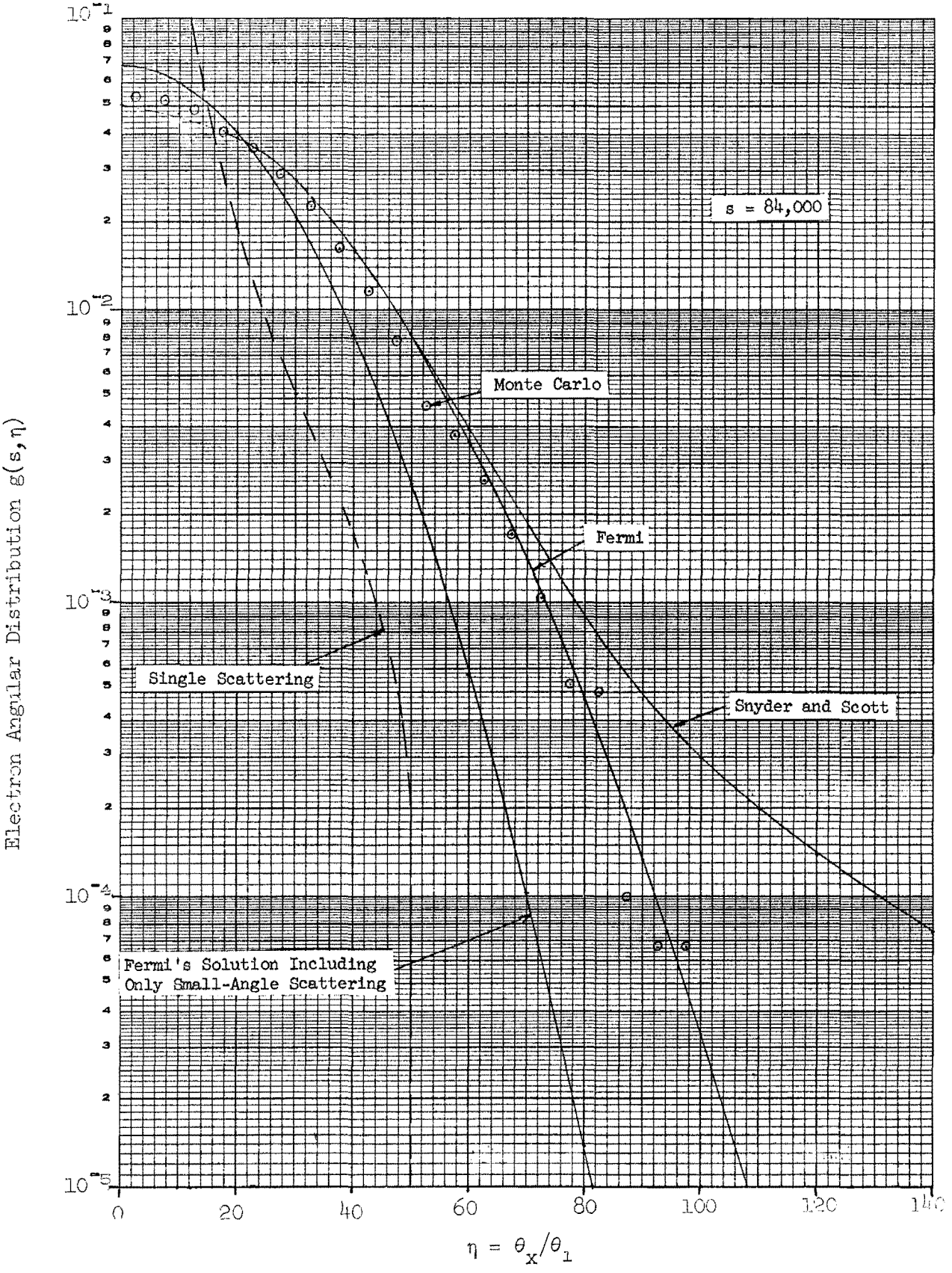

Fig. 6. Electron Angular Distribution in Lead at s = 84,000 (4.339 g/cm²) Resulting from a Monodirectional, 100-Mev Incident Beam of Electrons. Bremsstrahlung production and energy degradation by ionization collisions were not allowed.

Comparison with an Experiment

It is also of some interest to compare the calculation with one of the experiments of Kantz and Hofstadter.[12,13] In these experiments they obtained the spatial distribution of the energy deposited in various materials by 185-Mev electron-initiated showers. There is some doubt about the accuracy of the experimental data, however, as was pointed out previously.[2] It was shown, for example, that the longitudinal distribution of the energy deposition which was obtained by integrating over the measured radial distributions had far too high a maximum in comparison with the energy deposited at the source plane. Thus one must be careful not to rely too heavily on these data.

In the experiment the electron beam was collimated by a series of lead plates with aligned holes ranging up to a maximum diameter of 1/4 in. in the last few plates. The collimator apparently did not confine the beam to a small size, however, as can be seen in Fig. 7, which shows the measured radial distributions at various depths in tin. The experimental curve at zero depth clearly indicates the incident beam was quite extensive in comparison with the size of the collimator. For this reason, in all probability it was also far from normally incident on the slab in the radial wings.

To match the experiment as closely as possible, the calculation was performed with a beam with a radial distribution matching the measured zero depth curve. Since there was no way of choosing other than a monodirectional angular distribution for the beam from the data available, the calculation was limited to a normally incident source. This may account for some of the differences that appeared between the calculation and experiment.

In the calculation all photons in the shower that degraded below a cutoff energy of 2 Mev were considered to deposit their remaining

---

12. A. Kantz and R. Hofstadter, Nucleonics 12, March, p. 36 (1954).
13. A. D. Kantz, Electron-Induced Showers, Stanford University High-Energy Laboratory Report No. 17 (May, 1954).

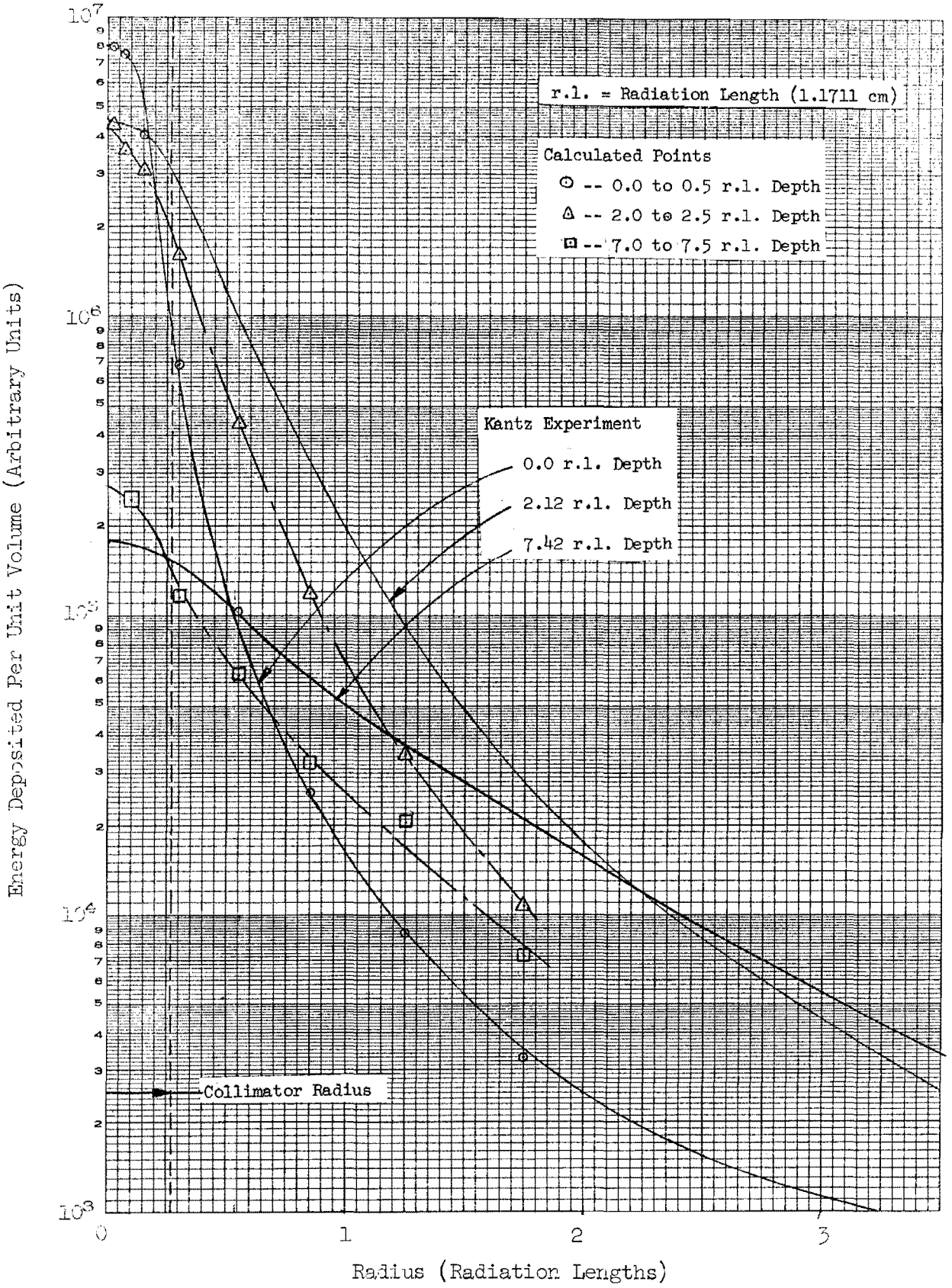

Fig. 7. Experimental and Calculated Radial Distributions of the Energy Deposited in Tin by Showers Initiated by Normally Incident, 185-Mev Electrons.

energy at the point where they dropped below the cutoff. The charged particles were treated in a similar fashion except that a 6-Mev cutoff energy was used. The energy deposited in each one-half radiation length depth and various radial intervals was calculated for comparison with the experiment. The calculated data points for the intervals 0 to 0.5, 2.0 to 2.5, and 7.0 to 7.5 radiation lengths are shown in Fig. 7 where the calculated data from the first interval has been normalized to the experimental data for zero depth. It will be seen that the calculated data for the first interval falls almost exactly on the zero depth experimental curve over the complete radius. The other calculated data are significantly different from the comparable experimental data. The differences, in part, can be attributed to the fact that the angular distribution of the source could not be duplicated.

Internal Distribution

1. F. S. Alsmiller
2. R. G. Alsmiller, Jr.
3. H. W. Bertini
4. E. P. Blizard
5. F. Clark
6. R. R. Coveyou
7. L. Dresner
8. W. A. Gibson
9. W. H. Jordan
10. F. B. K. Kam
11. W. E. Kinney
12. F. C. Maienschein
13. H. S. Moran
14. R. W. Peelle
15. S. K. Penny
16. D. K. Trubey
17-26. C. D. Zerby
27. W. Zobel
28-52. Laboratory Records
53. Laboratory Records, ORNL R.C.
54-55. Central Research Library
56. Document Reference Section
57-72. Division of Technical Information Extension (DTIE)
73. Research and Development (ORO)

External Distribution

74. Herman J. Schaefer; U.S. Naval School of Aviation, Pensacola, Fla.
75. S. P. Shen; New York University, University Heights, New York, N.Y.
76. E. A. Cosbie; Argonne National Laboratory, Argonne, Illinois
77-79. B. J. Moyer, R. Wallace, and W. Patterson; University of California Radiation Laboratory, Berkeley, California
80-81. K. G. Dedrick and W. K. H. Panofsky; Stanford Linear Accelerator Center, Stanford University, Stanford, California
82-86. H. DeStaebler, Jr.; Stanford Linear Accelerator Center, Stanford University, Stanford, California
87-91. R. F. Mozley; Stanford Linear Accelerator Center, Stanford University, Stanford, California
92. M. S. Livingston; Cambridge Electron Accelerator, 42 Oxford Street, Cambridge 38, Massachusetts
93. W. N. Hess; NASA, Goddard Space Flight Center, Greenbelt, Maryland
94. O. L. Tiffany; Bendix Systems Division, The Bendix Corporation, Ann Arbor, Michigan
95. R. L. Childers; University of Tennessee, Knoxville, Tennessee
96. A. Galonsky; Midwestern Universities, Research Association, 2203 University Avenue, Madison 5, Wisconsin
97-98. F. P. Cowan and S. J. Lindenbaum; Brookhaven National Laboratory, Upton, Long Island, New York
99. H. B. Knowles; Yale University, Sloane Laboratory, New Haven, Connecticut
100. R. B. Curtis, Indiana University, Bloomington, Indiana
101. J. S. Russ; Palmer Physical Laboratory, Princeton University, Princeton, New Jersey